IJST, Transactions of Mechanical Engineering, Vol. 37, No. M2, pp 217-232
Printed in The Islamic Republic of Iran, 2013

"Research Note"

ESTIMATION OF THE BREAKUP LENGTH FOR THE ANNULAR AND THE ROUND LIQUID JET USING LINEAR INSTABILITY ANALYSIS*

S.A. MAHDAVI [1], E. MOVAHEDNEJAD[2], F. OMMI[3**] AND S.M. HOSSEINALIPOUR[4]

[1]Imam Ali University, I. R. of Iran
[2]Islamic Azad University, Jolfa International Branch, I. R. of Iran
[3]Dept. of Mechanical Engineering, School of Engineering, Tarbiat Modares University, Tehren, I. R. of Iran
Email: fommi@modares.ac.ir
[4]Science and Technology University, Tehren, I. R. of Iran

Abstract– A linear instability analysis of an inviscid annular liquid sheet emanating from an atomizer subjected to inner and outer swirling air streams and a non-swirl round liquid jet has been carried out. The dimensionless dispersion equation that governs the instability was derived and was solved by Numerical method to investigate the effects of the liquid-gas swirl orientation on the maximum growth rate and its corresponding unstable wave number that produces the finest droplets. To understand the effect of air swirl orientation with respect to liquid swirl direction, four possible combinations with both swirling air streams with respect to the liquid swirl direction have been considered. Results show that at low liquid swirl Weber number a combination of co-inner air stream and counter-outer air stream has the largest most unstable wave number and shortest breakup length. The combination of inner and the outer air stream co-rotating with the liquid has the highest growth rate. Also, the results for round liquid jet and planar liquid sheet show that the linear theory accurately predicts the variation in breakup length with jet velocity.

Keywords– Annular sheet, round jet, atomization, linear analysis, instability, swirl

1. INTRODUCTION

Liquid atomization is of importance in numerous applications such as fuel injection in engines, gas turbine engines, industrial furnaces, agricultural sprays [1].

The instability and breakup of a liquid sheet is encountered in the liquid atomization process used in numerous applications including liquid fuel injection in combustion engines, spray drying of foods and detergents, and in manufacturing of pharmaceutical products [2]. The growth of disturbances on the jet liquid-air interface leads to sheet instability and breakup, and governs the characteristics of the resulting spray. These characteristics play an important role in determining the subsequent heat/mass transport and phase change processes. For example, the liquid sheet instability and breakup in the fuel atomizer in combustion engines determines the mean drop size in the fuel spray and has direct impact on combustion efficiency, pollutant emissions and combustion instability. Due to good atomization characteristics and low liquid pressure requirements, air-blast atomizers are being considered in many applications. In an air-blast atomizer, the kinetic energy of the high-speed swirling airstreams is used to breakup the liquid sheet. The liquid exits the air-blast atomizer as an annular sheet and is subjected to swirling inner and outer air streams [3]. The presence of the atomizing air leads to shorter breakup length and enhances liquid air mixing [4, 5].

*Received by the editors November 19, 2009; Accepted September 25, 2013.
**Corresponding author

The stability of liquid jets and sheets has received much attention since the classical studies of Rayleigh and Squire. For authoritative reviews of liquid sheet and jet instability and breakup, readers are referred to a recent monograph by Lin [6] and reviews by Sirignano and Mehring [7].

The investigation of liquid sheet breakup and the subsequent spray formation is first conducted with a two-dimensional planar nozzle originally designed by Jazayeri and Li [9]. This two-dimensional planar nozzle has an aspect ratio 100:1at the nozzle exit, and hence produces a liquid sheet at the nozzle exit with the thickness of 0.254 mm and two air flow outlets, located on either side of the liquid channel. A set of honeycomb and fine screens are placed upstream of the nozzle contraction for both the flow passages to reduce the turbulence level in the flow.

It is well established that the forces acting on a liquid gas interface including surface tension, pressure, inertia force, centrifugal force and viscous force result in the growth of disturbances and instability of liquid sheet which eventually breaks up into ligaments. The liquid sheet instability is responsible for spray formation and determines the resultant spray characteristics such as droplet size, velocity and their distributions. In an air-blast atomizer, all the three streams, i.e., the liquid, the inner air and the outer air, may have swirl velocity components, in addition to axial motion. Furthermore, with both liquid and air swirling, the effect of swirl direction should be considered.

According to the paper results, for a certain range of Weber number the shortest breakup lengths were obtained with both the inner and the outer air streams co-rotating with the liquid stream. They also show that the effect of liquid and air swirl is different in another range of Weber numbers. The model is also simplified for a round liquid jet and the dispersion equation of wave growth rate similar to Weber formulation is derived. Both models are validated by comparison with earlier analytical studies as well as with experimental data of sheet breakup length available in literature.

The main objective of this paper is to develop and investigate the ability of linear instability model to predict breakup length of three different sprays, annular liquid sheet, round liquid jet and planner liquid sheet.

2. LINEAR INSTABILITY ANALYSIS OF ANNULAR LIQUID SHEET

a) Model assumptions

The stability model considers a swirling inviscid annular liquid sheet subject to swirling airstreams. Gas phases are assumed to be inviscid and incompressible.

The basic flow velocities for liquid, inner gas and outer gas are assumed to be $(U_1,0, A_1/r)$, $(U_i,0, \Omega r)$, $(U_o,0, A_o/r)$ respectively and $A_o, A_1 (m^2/s)$ are Vortex Strength and $\Omega\ (1/s)$ is Angular velocity.

Due to the swirling coaxial flow effect, centrifugal forces act on the annular liquid sheet. Additionally, inner and outer pressure forces are another type of forces acting on the inner and outer interfaces respectively. Furthermore, the liquid surface tension forces play an important role in preventing the formation of a new surface. The sum of these forces determines whether the annular liquid sheet is going to breakup or remains stable.

b) Linearized disturbance equations

The governing equations for inviscid annular fluid flows are the continuity and Euler equations that in cylindrical coordinate system are:

Continuity equation:

$$\frac{\partial U}{\partial x}+\frac{V}{r}+\frac{\partial V}{\partial r}+\frac{1}{r}\frac{\partial W}{\partial \theta}=0 \tag{1}$$

Momentum equations:

$$\frac{\partial U}{\partial t}+U\frac{\partial U}{\partial x}+V\frac{\partial U}{\partial r}+\frac{1}{r}W\frac{\partial U}{\partial \theta}=-\frac{1}{\rho}\frac{\partial P}{\partial x} \tag{2}$$

$$\frac{\partial V}{\partial t}+U\frac{\partial V}{\partial x}+V\frac{\partial V}{\partial r}+\frac{1}{r}W\frac{\partial V}{\partial \theta}-\frac{W^2}{r}=-\frac{1}{\rho}\frac{\partial P}{\partial r} \tag{3}$$

$$\frac{\partial W}{\partial t}+U\frac{\partial W}{\partial x}+V\frac{\partial W}{\partial r}+\frac{1}{r}W\frac{\partial W}{\partial \theta}+\frac{VW}{r}=-\frac{1}{\rho r}\frac{\partial P}{\partial \theta} \tag{4}$$

The disturbances are assumed to have the forms

$$(u,v,w,p')=(\hat{u}(r),\hat{v}(r),\hat{w}(r),\hat{p}'(r))e^{i(kx+n\theta-\omega t)} \tag{5}$$

Where ^ indicates the disturbance amplitude which is a function of r only. For the temporal analysis, the wave number k and n are real while frequency ω is complex. The imaginary part of $\omega=\omega_r+i\omega_i$ reflects the growth rate of the disturbance. The displacement disturbances at the inner and outer interfaces are

$$\eta_j(x,\theta,t)=\hat{\eta}_j e^{i(kx+n\theta-\omega t)} \quad ; \quad j=i,o \tag{6}$$

To obtain the linearized disturbance equations, let

$$U=\overline{U}+u \ , \ V=v \ , \ W=\overline{W}+w \ , \ p=P+p' \tag{7}$$

Where the over bar represents the assumed mean flow quantities and the prime indicates disturbance. The linearized disturbed equations for the liquid phase are written in vector form as

$$\nabla.\vec{v}=0 \tag{8}$$

$$\left(\frac{\partial}{\partial t}+\frac{A_l}{r^2}\frac{\partial}{\partial \theta}+U_l\frac{\partial}{\partial x}\right)\vec{v}=-\frac{1}{\rho}\nabla p_l' \tag{9}$$

The linearized disturbed equations for the inner and outer air are written in component form as:

Continuity equation

$$\frac{\partial u}{\partial x}+\frac{v}{r}+\frac{\partial v}{\partial r}+\frac{1}{r}\frac{\partial w}{\partial \theta}=0 \tag{10}$$

Momentum equations

$$\frac{\partial u}{\partial t}+U_j\frac{\partial u}{\partial x}+\frac{W_j}{r}\frac{\partial u}{\partial \theta}=-\frac{1}{\rho_j}\frac{\partial p_j'}{\partial x} \tag{11}$$

$$\frac{\partial v}{\partial t}+U_j\frac{\partial v}{\partial x}+\frac{W_j}{r}\frac{\partial v}{\partial \theta}-\frac{2W_j w}{r}=-\frac{1}{\rho_j}\frac{\partial p_j'}{\partial r} \tag{12}$$

$$\frac{\partial w}{\partial t}+U_j\frac{\partial w}{\partial x}+v\frac{\partial W_j}{\partial r}+\frac{W_j}{r}\frac{\partial w}{\partial \theta}+\frac{W_j v}{r}=-\frac{1}{\rho_j r}\frac{\partial p_j'}{\partial \theta} \tag{13}$$

Where

$$j=i,o \ \ and \ \ W_i=r\Omega, W_o=A_o/r \tag{14}$$

Boundary conditions must be applied at the liquid interface. The first boundary condition is the kinematic condition and can be expressed for the inner interface

at $r=R_a$ as

$$v_i=\frac{D\eta_i}{Dt}=\frac{\partial \eta_i}{\partial t}+U_i\frac{\partial \eta_i}{\partial x}+\Omega\frac{\partial \eta_i}{\partial \theta} \qquad at \qquad r=R_a \tag{15}$$

$$v_l = \frac{D\eta_i}{Dt} = \frac{\partial \eta_i}{\partial t} + U_l \frac{\partial \eta_i}{\partial x} + \frac{A_l}{r^2}\frac{\partial \eta_i}{\partial \theta} \quad at \quad r = R_a \tag{16}$$

And for the outer interface at $r = R_b$ as

$$v_o = \frac{D\eta_o}{Dt} = \frac{\partial \eta_o}{\partial t} + U_o \frac{\partial \eta_o}{\partial x} + \frac{A_o}{r^2}\frac{\partial \eta_o}{\partial \theta} \quad at \quad r = R_b \tag{17}$$

$$v_l = \frac{D\eta_o}{Dt} = \frac{\partial \eta_o}{\partial t} + U_l \frac{\partial \eta_o}{\partial x} + \frac{A_l}{r^2}\frac{\partial \eta_o}{\partial \theta} \quad at \quad r = R_b \tag{18}$$

The second boundary condition considers the balance between the surface stresses on both sides of the liquid-gas interface, including the pressure jump across the interface due to surface tension and viscous forces. This boundary condition is known as the dynamic boundary condition and is given by

$$p_l' - p_i' = \sigma\left(\frac{\eta_i}{R_a^2} + \frac{\partial^2 \eta_i}{\partial x^2} + \frac{1}{R_a^2}\frac{\partial^2 \eta_i}{\partial \theta^2}\right) + \rho_l \Omega^2 R_a \eta_i - \frac{\rho_l A_l^2 \eta_i}{R_a^3} \quad at\, r = R_a \tag{19}$$

$$p_l' - p_o' = -\sigma\left(\frac{\eta_o}{R_b^2} + \frac{\partial^2 \eta_o}{\partial x^2} + \frac{1}{R_b^2}\frac{\partial^2 \eta_o}{\partial \theta^2}\right) + \frac{\rho_o A_o^2 \eta_o}{R_b^3} - \frac{\rho_l A_l^2 \eta_o}{R_b^3} \quad at\, r = R_b \tag{20}$$

c) Pressure disturbance inside the liquid sheet

The Pressure disturbance inside the annular liquid sheet is the solution to Eq. (8, 9). Substituting Eq. (5) into Eq. (8, 9), and after some simplifications we obtain the following equations:

$$\frac{\hat{v}}{r} + \frac{d\hat{v}}{dr} + \frac{1}{r}(in)\hat{w} + ik\hat{u} = 0 \tag{21}$$

$$\frac{1}{k}\left(-\omega + kU_l + \frac{nA_l}{r^2}\right)\hat{u} = -\frac{1}{\rho_l}\hat{p}_l \tag{22}$$

$$i\left(-\omega + kU_l + \frac{nA_l}{r^2}\right)\hat{v} - \frac{2A_l}{r^2}\hat{w} = -\frac{1}{\rho_l}\frac{d\hat{p}_l}{dr} \tag{23}$$

$$\frac{r}{n}\left(-\omega + kU_l + \frac{nA_l}{r^2}\right)\hat{w} = -\frac{1}{\rho}\hat{p}_l \tag{24}$$

From Eq. (22) and Eq. (24) we get

$$\hat{w} = \frac{n}{kr}\hat{u} \tag{25}$$

Differentiating Eq. (24) with respect to r and utilizing Eq. (23) leads to the following simplified equation

$$\hat{v} = \frac{1}{in}\left(\hat{w} + r\frac{d\hat{w}}{dr}\right) \tag{26}$$

Substituting Eq. (25) into Eq. (26) leads to the following equation

$$\hat{v} = -\frac{i}{k}\frac{d\hat{u}}{dr} \tag{27}$$

After substituting Eq. (25) and (27) into Eq. (21), the continuity equation becomes

$$\frac{d^2\hat{u}}{dr^2} + \frac{1}{r}\frac{d\hat{u}}{dr} - \left(\frac{n^2}{r^2} + k^2\right)\hat{u} = 0 \tag{28}$$

The above equation is a Bessel equation which has a solution of the form:

$$\hat{u}(r) = c_1 I_n(kr) + c_2 K_n(kr) \tag{29}$$

After substituting Eq. (29) into Eq. (22):

$$p_l' = \frac{\rho_l}{k}\left(\omega - kU_l - \frac{nA_l}{r^2}\right)\left(c_1 I_n(kr) + c_2 K_n(kr)\right)e^{i(kx+n\theta-\omega t)} \tag{30}$$

Substituting Eq. (5) and (6) into the Kinematic boundary conditions for the swirling liquid Eq. (16) and (18) and utilizing Eq. (27) c_1, c_2 are obtained [9].

d) Pressure disturbance inside the inner and outer air

The pressure disturbances can be obtained inside the inner air and outer air similar to liquid after solving the equations to form the following, respectively [9]:

$$P_i' = \frac{\rho_i\left[\left(-\omega + kU_i + n\Omega\right)^2 - 4\Omega^2\right]\left(-\omega + kU_i + n\Omega\right)\hat{\eta}_i I_n(k_1 r)e^{i(kx+n\theta-\omega t)}}{\left(-\omega + kU_i + n\Omega\right)k_1 I_n'(k_1 R_a) + \dfrac{2n\Omega}{R_a} I_n(k_1 R_a)} \tag{31}$$

$$p_o' = \frac{\rho_o}{k}\left(\omega - kU_o - \frac{nA_o}{R_b^2}\right)\left(\omega - kU_o - \frac{nA_o}{r^2}\right)\hat{\eta}_o \frac{K_n(kr)}{K_n'(kR_b)} e^{i(kx+n\theta-\omega t)} \tag{32}$$

Where $I_n(kr), K_n(kr)$ are the n_{th} order modified Bessel Function of the first and the second kind respectively.

The dispersion equation is obtained by substituting the pressure disturbances inside the liquid and the gas phases into the dynamic boundary conditions at the two interfaces. In order to determine the effect of the various forces, properties of fluids and other geometric parameters, the non-dimensional form of final equations are made by introducing the following dimensionless parameters:

$$\begin{aligned}
&We_i = \frac{\rho_i U_i^2 R_b}{\sigma} && We_0 = \frac{\rho_o U_o^2 R_b}{\sigma} && We_l = \frac{\rho_l U_l^2 R_b}{\sigma} \\
&We_{si} = \frac{\rho_i \Omega^2 R_b^3}{\sigma} && We_{so} = \frac{\rho_o A_o^2}{\sigma R_b} && We_{sl} = \frac{\rho_l A_l^2}{\sigma R_b} \\
&g_i = \frac{\rho_i}{\rho_l} && g_o = \frac{\rho_o}{\rho_l} && h = \frac{R_a}{R_b} \\
&\bar{k} = kR_b && \varpi = \frac{\omega R_b}{U_l}
\end{aligned} \tag{33}$$

The fourth order dispersion equation is obtained and can be written in the form below. The final dispersion equation can be solved numerically using the secant method.

$$a_1\overline{\omega}^4 + a_2\overline{\omega}^3 + a_3\overline{\omega}^2 + a_4\overline{\omega} + a_5 = 0 \tag{34}$$

With substituting $\overline{\omega}$ and its corresponding most unstable wave number into Eqs. (35, 36, 37), breakup length L_b, ligament and drop diameter d_L, d_D are obtained [10, 11]:

$$\mathrm{L_b} = \frac{12 \,.\, \mathrm{R_b}}{\overline{\omega}} \tag{35}$$

$$\mathrm{d_L} = \sqrt{\frac{16 \,.\, \mathrm{h_s} \,.\, R_b}{\overline{\mathrm{K}}}} \tag{36}$$

$$\mathrm{d_D} = 1.88\ \mathrm{d_L} \tag{37}$$

3. LINEAR INSTABILITY ANALYSIS OF NON-SWIRL ROUND LIQUID JET

Rayleigh found that disturbances initially present in the stream grow exponentially [exp (wt)], where w is the growth rate factor. Weber [12] extended Rayleigh's analysis to jets of viscous liquids and obtained the following equation for wave growth rate on round liquid jet:

$$w = -\frac{3}{2}\frac{\eta}{\rho}\left(\frac{2\pi}{\lambda}\right)^2 + \left\{\left\{\frac{9}{4}\left(\frac{\eta}{\rho}\right)^2\left(\frac{2\pi}{\lambda}\right)^4 + \frac{\sigma r^2}{2\rho r^3}\left(\frac{2\pi}{\lambda}\right)^2\left[1-\left(\frac{2\pi r}{\lambda}\right)^2\right]\right\}\right\}^{1/2} \tag{38}$$

Following the previous approach and simplifying constraint equations for round liquid jet, the growth rate formulation for inviscid liquid jet in quiescent air can be obtained easily. In this circumstance all formulation related to inner gas will be omitted. Besides, as both liquid and outer gas flow are non-swirl, the swirl parameters A_l and A_o are neglected. The liquid jet considers axis metric and consequently $n \to 0$. Considering the above assumptions the pressure disturbance inside the liquid jet and outer gas is obtained as follows:

$$p'_l = \frac{\rho_l}{k}(\omega - kU_l)(c_1 I_n(kr))e^{i(kx-\omega t)}$$
$$c_1 = \eta_0 \frac{(w - kU_l)}{I'(KR_b)} \tag{39}$$

$$p'_o = \frac{\rho_o}{k}(\omega - kU_o)(\omega - kU_o)\hat{\eta}_o \frac{K_n(kr)}{K'_n(kR_b)}e^{i(kx-\omega t)} \tag{40}$$

Also, equation 20 changes to:

$$p'_l - p'_o = -\sigma\left(\frac{1}{R_b^2} - k^2 - \frac{n^2}{R_b^2}\right)\hat{\eta}_0 \, at \, r = R_b \tag{41}$$

Substituting Eq. (39) and (40) into Eq. (41) leads to the final equation

$$w^2\left(1 - \frac{\rho_o}{\rho_l}\frac{I'_n}{I_n}\frac{K_n}{K'_n}\right) = -\frac{\sigma k}{\rho_l R_b^2}(1 - R_b^2 k^2)\frac{I'_n}{I_n} \tag{42}$$

The second order dispersion equation as the final dispersion equation was solved numerically using the secant method.

According to the Reitz's relation [13] the breakup time and consequently breakup length for round liquid jet can be estimated using the following relations:

$$\tau = \frac{3.778\, B_1 r_o}{\omega_s \lambda_s} \qquad B_1 = 20$$
$$L_b = \tau_s U_l \tag{43}$$

4. VALIDATION

For each pair of dimensionless parameters $(n, \bar{k})$, the fourth order non-linear dispersion equation has been solved for the root $\bar{\omega} = \omega R_b / U_l$ using secant method. Maximum imaginary part of complex roots represents the maximum growth rate of the disturbance.

As a validation of the results, both analytical (Ibrahim) and experimental data (Shen) of previous works have been used in the same liquid jet and inner and outer gas specifications [14, 15]. Figure 1-a

shows the comparison of equation solving results for different wave numbers with a linear analysis for the annular jet [16].

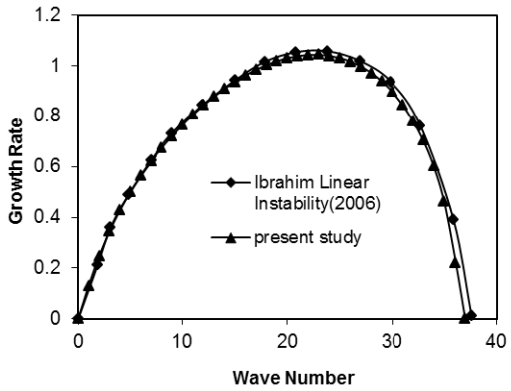

Fig. 1a: comparison of results with linear analysis of Ibrahim et al. [16] for different wave numbers.
$We_l = 10000, We_i = 0, We_o = 70, We_s = 500,$
$We_{si} = We_{so} = 0,\ g_i = g_o = 0.0123,\ h = 0.667, n = 0$

Figure 1-b shows a comparison of linear, nonlinear and experimental results for breakup length of liquid sheet for different gas relative velocities. The effect of viscosity has been neglected in linear analysis and causes the difference between linear and experimental results, since the liquid viscosity causes the breakup length to increase. Furthermore, the trend of breakup length variation is the same for all of them. It is important to mention that linear theory can predict breakup of an annular sheet for small level initial disturbances and the developed nonlinear model is necessary to accurately determine the breakup length for high initial disturbances. [14]

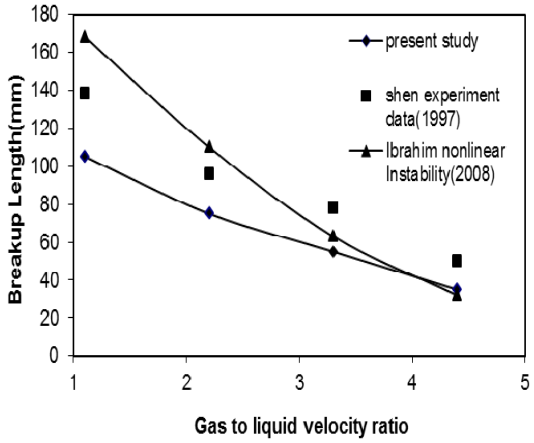

Fig. 1b. Comparison of linear, nonlinear and experimental results for breakup length for different gas relative velocities $g_i = g_o = 0.0012, h = 0.95, n = 0$

Real solutions of the dispersion equation (42) for linear instability analysis of a round liquid jet are obtained for wave numbers in the range of 0 to 1. The present analysis is validated by comparing the predictions of wave growth rate with Weber theory [12] together with the experimental result of Bruce [17] and is shown in Fig. 2a.

Further validation of the model is carried out by comparing measurements of breakup length with empirical correlations available in the literature for jet breakup in stationary gas. The effect of axial liquid velocity on the liquid jet break up length in stationary gas is presented in Fig. 2b. For each value of the

Weber number, the disturbance wave numbers with the highest growth rate are obtained. Using Reitz's relation in Eq. (43) the breakup length can be calculated as the product of the axial velocity of the jet and the breakup time. The characteristics of the data used in literature are presented in Table 1.

According to the Fig. 2b, as the jet velocity increases, a linear increase is observed in the breakup length during the Rayleigh regime. Thereafter the breakup length enters a nonlinear regime, leading to a maximum at a critical velocity (V_c). Mansour and Chigier [18] have shown that turbulence may play a role only for velocities higher than Vc. As the results are restricted to jets emerging in air at atmospheric pressure with velocities corresponding to Rayleigh and first wind induced regimes, no turbulence is to be considered [19]. The figure shows acceptable agreement between experiment and linear theory, although linear theory predicts the longer breakup length. So the result agrees with the Kalaaji et al. [20] data that the linear theory accurately predicts the variation in breakup length with jet velocity. However, it should not be concluded that linear analysis fully describes the jet behavior.

Table 1. Characteristics of the literature data analysis of liquid jet

	Bruce[16]	Sallam [21]
Viscosity (mPas)	2.62	0.894
Surface Tension (N/m)	0.052	0.072
Density (g/l)	1022	997
Nozzle Radius (micron)	20	1.9
Re	169	

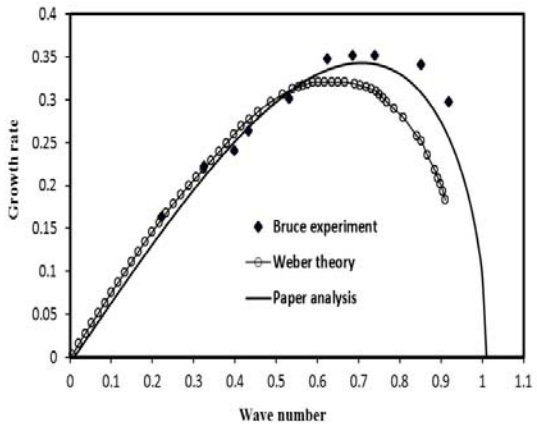

Fig. 2a. Growth rates versus wave number of liquid jet

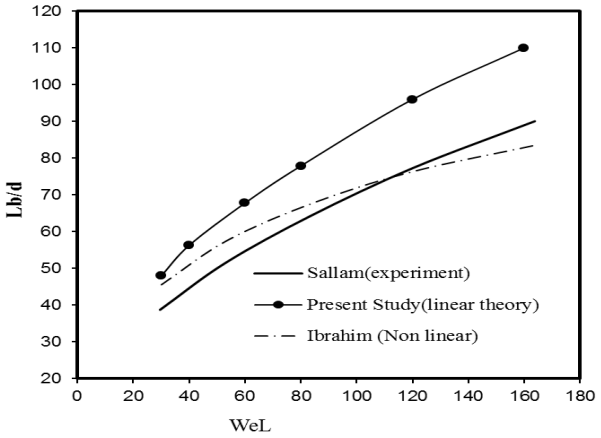

Fig. 2b. Dimensionless breakup length versus axial liquid jet Weber number for n = 0.

For verification of the results, spray produced by an air-blast atomizer in this study was compared with experiment data (The PDPA measurement) of planar nozzle and the theoretical prediction by Kim et al. [22]. Table 2 presents the flow conditions and Table 3 presents breakup length at the nozzles exit.

Table 2. Exit flow conditions for the planar nozzle with liquid density ρl=998.2 kg/m3, gas density ρg=1.204 kg/m3 and surface tension σ=7.36×10-2 N/m2

Case	U_l(m/s)	U_g(m/s)	We_l
I	1.0	32.6	1.72
II	2.0	28.0	6.89
III	1.0	28.0	1.72
IV	2.0	32.6	6.89

Table 3. Estimates of breakup length

Lb(mm)		
Experiment	Kim Prediction [22]	Present Study
3	3	2.91
6	6	6.1
3	3	2.98
5	5	5.18

It is observed that, overall the predicted distribution matches well with the experimental data and the results also show good agreement [23].

5. RESULTS AND DISCUSSION

The instability of the annular liquid sheet changes significantly when swirl is applied to the air stream which is illustrated in Figures 3-a, 3-b and 3-c. When the inner and outer gases are not swirling, the axisymetric mode (n=0) dominates by having the highest growth rate in the disintegration process (Fig. 3-a).

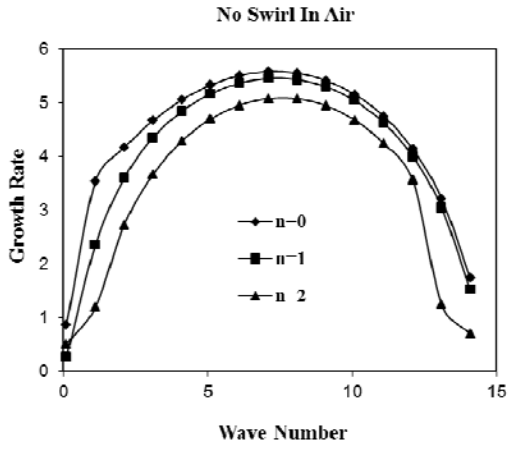

Fig. 3a. Effects of air swirl on dispersion diagram at We_l=35, We_i=15, We_o=15, h = 0.9

When swirl motion is applied on the inner or outer air streams, the maximum growth rate and its corresponding most unstable wave number increases with the increase of the annular liquid sheet helical mode as shown in Figure 3-b and Fig. 3c respectively. Moreover, the increase in the maximum growth rate and the most unstable wave number caused by the inner air swirl is higher than the increase caused by the outer air swirl for the first three helical modes. This shows that the inner air swirl is more efficient than the outer one and a shorter breakup length and finer droplet diameters are produced using the inner gas flow.

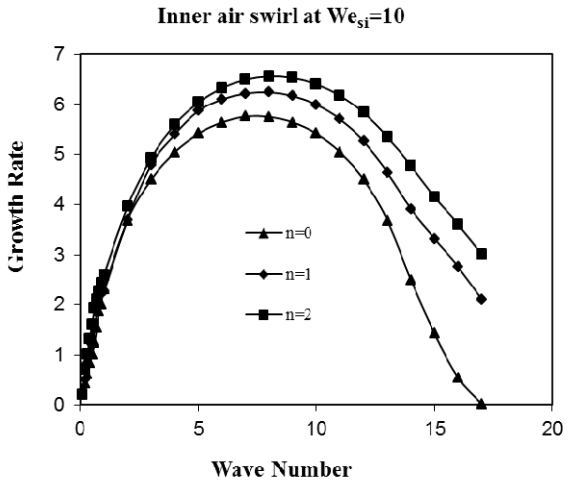

Fig. 3b. Effects of inner air swirl on dispersion diagram at We_l=35, We_i=15, We_o=15, We_{si}=10, h = 0.9

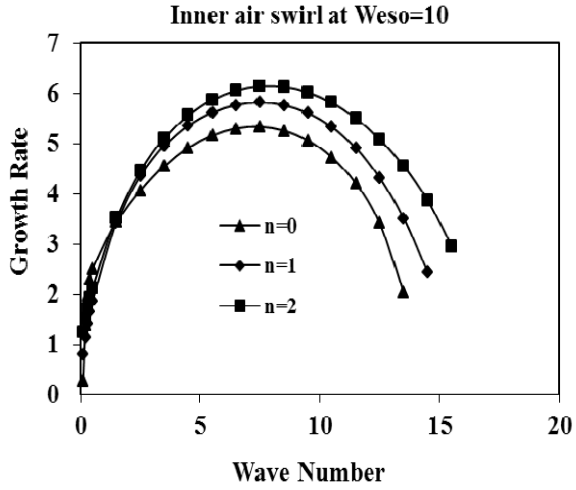

Fig. 3c. Effects of outer air swirl on dispersion diagram at We_l=35, We_i=15, We_o=15, We_{so}=10, h = 0.9

Figure 4 illustrates the effect of second helical mode i.e. n=2 on the liquid sheet disintegration under the four different orientation categories. As shown in Fig. 4 the most unstable wave number corresponding to the maximum growth rate occurs when the outer air rotates in the opposite direction (counter swirl) and the inner air rotates in the same direction with respect to the liquid swirl orientation. On the other hand, the least unstable wave number corresponding to the maximum growth rate occurs when the inner air rotates in the opposite direction and the outer air rotates in the same direction with respect to liquid swirl orientation. As Fig. 4 shows, the maximum growth rate for co-inner air flow is higher than the counter-inner one.

According Eq. (36) the produced droplets size is inversely related to the most unstable wave number. So, it can be concluded that the co-inner and counter-outer swirl configuration produces the finest droplets, which shows an agreement with the earlier analytical results [3]. Moreover, the shortest breakup length can be achieved when co inner and co outer air streams exist because of its maximum growth rate (Eq. 35).

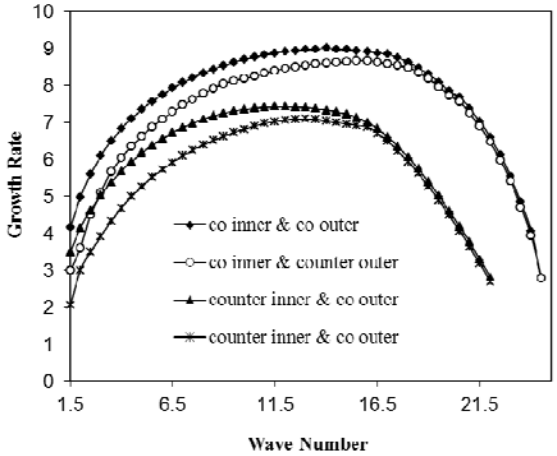

Fig. 4. Effect of air swirl orientation categories on the dispersion diagram at We_l=35, We_i=25, We_o=15, We_s=0.01, We_{si}=10, We_{so}=10, h=0.9, g_i and g_o=0.00129

The influence of the four different swirl orientation categories on the disintegration process appears when they are applied to the second annular liquid sheet helical mode as it is shown in Figs. 5 and 6.

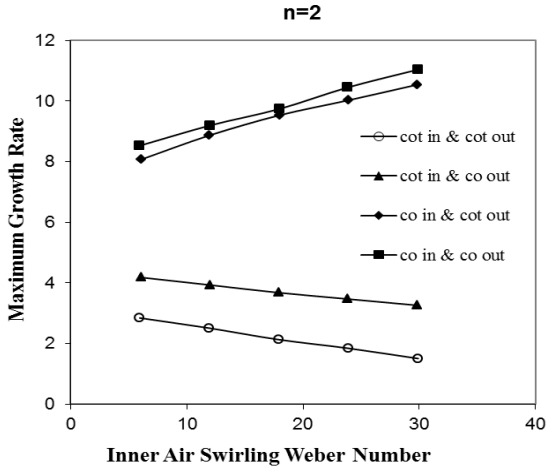

(a)

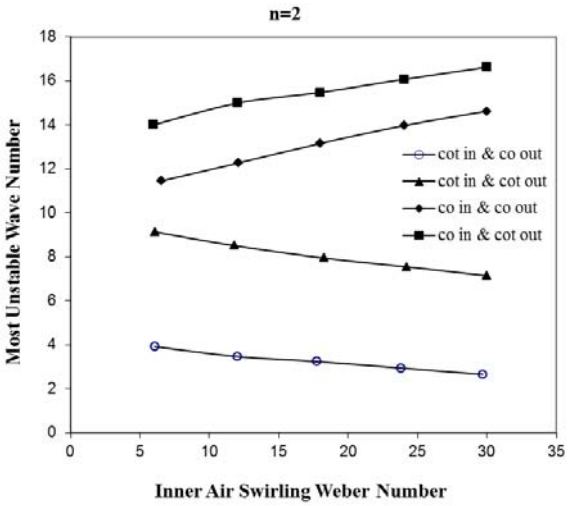

(b)

Fig. 5. Effect of the swirling inner air on the disintegration of the second helical annular liquid sheet at We_l=35, We_i=25, We_o=15, We_s=0.01, We_{so}=10, h=0.9

As it is shown, the inner air orientation defines the trend of variations. The increase of the inner air swirl velocity in the co-inner gas tends to increase the disturbance maximum growth rate and its most unstable wave number, which speeds up the breakup process and produces finer spray droplets. The increase of the inner air swirl velocity has an inverse effect for counter-inner gas flow (Figs. 5a and 5b).

As shown in Figs. 6a and 6-b increasing the outer-air swirl strength when it is applied on the second helical mode increases the most unstable wave number. Utilizing the co-inner and counter-outer swirl category produces the finest spray droplet diameters as it corresponds to the highest most unstable wave number among all the swirl orientation categories.

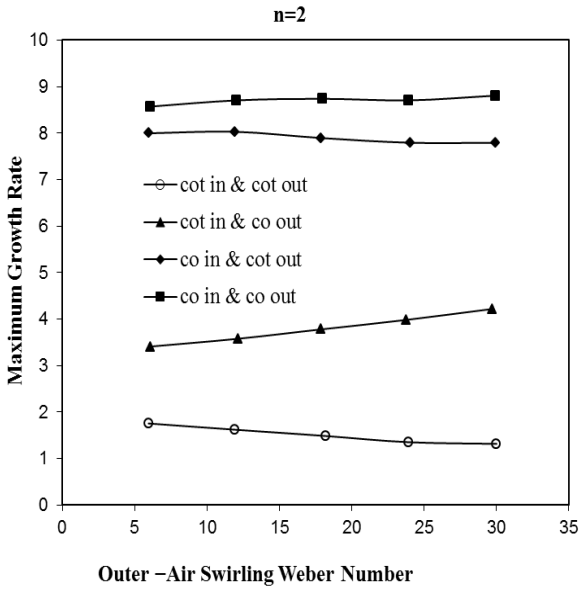

(a)

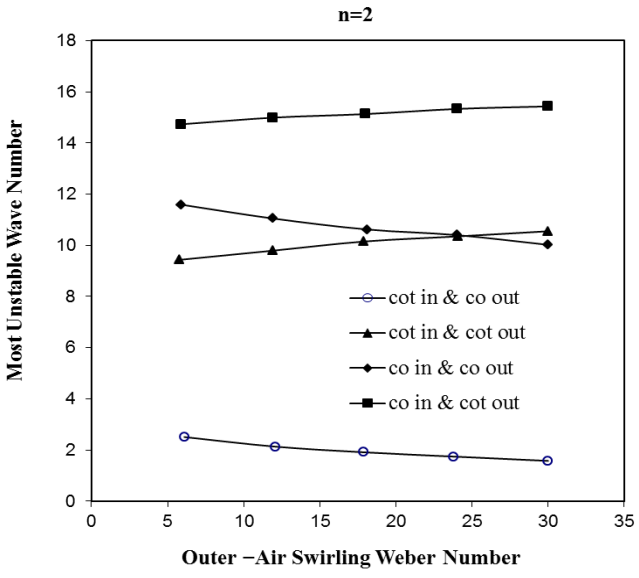

(b)

Fig. 6. Effect of the swirling outer air on the disintegration of the second helical annular liquid sheet at We_l=35, We_i=25, We_o=15, We_s=0.01, We_{si}=10, h=0.9

Figures 7 and 8 show the effect of air swirl orientation categories on the breakup length and drop diameter. As it is seen in Fig. 7 shorter breakup length can be achieved using co-inner gas flow orientation rather than counter-inner one.

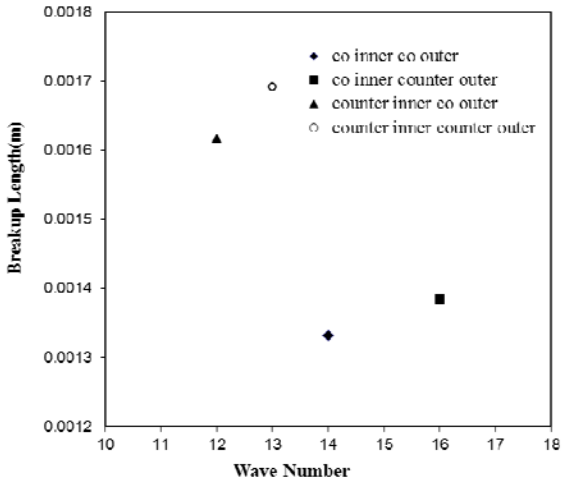

Fig. 7. Effect of air swirl orientation categories on the breakup length at We_l=35, We_i=25, We_o=15, We_s=0.01, We_{si}=10, We_{so}=10, h=0.9, g_i and g_o=0.00129

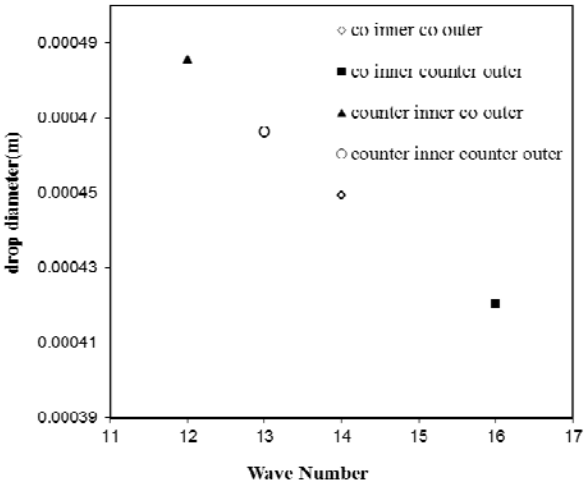

Fig. 8. Effect of air swirl orientation categories on the drop diameter at We_l=35, We_i=25, We_o=15, We_s=0.01, We_{si}=10, We_{so}=10, h=0.9, g_i and g_o=0.00129

6. CONCLUSION

A linear instability analysis of an inviscid swirl annular liquid sheet and a non-swirl round liquid jet has been carried out to investigate the accuracy of linear prediction of breakup length for the low perturbed liquid jet. Also, a dimensionless parametric study has been conducted to determine the effect of the inner and outer air swirl orientations on the instability of the annular liquid sheet for the second helical mode. The results show that the inner air swirl has a significant effect on instability of liquid sheet. Also, the highest most unstable wave number is produced by the co-inner and counter-outer mode among the four different swirl orientation categories, which means that the finest droplets are by this category. Co-inner and co-outer air stream produces the highest maximum growth rate. The growth rate can be related to the breakup length of the liquid sheet and a higher growth rate is indicated by a shorter breakup length. Also, to increase the growth rate, inner air swirl has a dominant effect compared to outer air swirl. The method used for analyzing annular sheet was simplified for a non-swirl round liquid jet and the result was compared to Weber theory and experimental data. It shows that the linear theory accurately predicts the breakup length and it's variation with jet velocity for the low perturbed liquid jet.

NOMENCLATURE

A	vortex Strength m^2/s or $1/s$	V	mean radial velocity (m/s)
g	gas-to-liquid density ratio	v	disturbance radial velocity (m/s)
h	ratio of inner and outer radius	W	mean tangential velocity (m/s)
I_n	n_{th} order modified Bessel function of first kind	We	weber number ($\rho_l U^2 R_b/\sigma$)
K_n	n_{th} order modified Bessel function of second kind	w	disturbance tangential velocity (m/s)
$k = 1/\lambda$	axial wave number ($1/m$)	***Greek symbols***	
n	circumferential wave number (Rad)	η	displacement disturbance (m)
P	mean pressure (N/m^2)	ρ	fluid density (kg/m^3)
p'	disturbance pressure (N/m^2)	σ	surface tension (kg/s^2)
R_a	inner diameter of liquid sheet (m)	ω	temporal growth rate ($1/s$)
R_b	outer diameter of liquid sheet (m)	**Subscripts**	
L_b	breakup length	i	inner air
d_L	ligament diameter	l	liquid phase
d_D	drop diameter	o	outer air
r	radial coordinate (m)	s	based on swirling component
t	time (s)	si	inner air swirling
x	axial coordinate (m)	so	outer air swirling
U	mean axial velocity (m/s)	sl	liquid phase swirling
u	disturbance axial velocity (m/s)		

REFERENCES

1. Herrero, P., Martin Del Valle., E. M. & Galan, M. A. (2007). Instability study of a swirling annular liquid sheet of polymer produced by air-blast atomization Edgar, p. 133.
2. Tahavvor, A. R. (2013). Experiment and numerical study of a turbulent axisymmetric jet impinging onto a circular cylinder in offset and non-offset situations. *Iranian Journal of Science and Technology, Transactions of Mechanical Engineering*, Vol. 37, No. M1, pp. 63-70
3. Ibrahim, A. A. & Jog, M. A. (2006). Effect of liquid and air swirl strength and relative rotational direction on the instability of an annular liquid sheet. *Acta Mechanica*, Vol. 186, pp. 113–133.
4. Carvalho, I. S. & Heitor, M. V. (1998). Liquid film break-up in a model of a prefilming airblast nozzle. Exp. Fluids 24, pp. 408–415.
5. Lavergne, G., Trichet, P., Hebrard, P. & Biscos, Y. (1993). Liquid sheet disintegration and atomization process on a simplified airblast atomizer. *J. Engng. Gas Turbines Power*, Vol. 115, pp. 461–466.
6. Lin, S. P. (2003). *Breakup of liquid sheets and jets*. Cambridge University Press.
7. Sirignano, W. A. & Mehring, C. (2000). Review of theory of distortion and disintegration of liquid streams. *Prog. Energy Combustion Sci*., Vol. 26, pp. 609–655.
8. Jazayeri, S. A. & Li, X. (2000). Structure of liquid-sheet sprays. *Part. Part. Syst. Charact*., Vol. 17, pp. 56-65.
9. Askari Mahdavi, S. (2009). Thesis of M.S in mechanical engineering, Tarbiat Modares University.
10. Senecal, P. K., Schmidt, D. P., Nouar, I., Rutland, C. J. & Reitz, R. D. (1999). Modeling high-speed viscous liquid sheet atomization. Corradini, *International Journal of Multiphase Flow*, Vol. 25, pp. 1073-1097.
11. Dombrowski, N. & Johns, W. R. (1963). The aerodynamic instability and disintegration of vicious liquid sheets. *Chem. Eng. Science*, Vol. 18, pp. 203 –214.

12. Weber, C. (1931). Zum zerfall eines fliissigkeitsstrahles. *Z. Angew. Math. Mech.*, Vol. 11, p. 136.
13. Reitz, R. D. (1978). Modeling atomization processes in high- pressure vaporizing sprays atomization and spray technology. Vol. 3, pp. 309-337.
14. Shen, J. & Li, X. (1996). Instability of an annular viscous liquid jet. *Acta Mech*., Vol. 114, pp. 167–183.
15. Ibrahim, A. A. & Jog, M. A. (2008). Nonlinear instability of an annular liquid sheet exposed to gas flow. *International Journal of Multiphase Flow*, Vol. 34, pp. 647–664.
16. Ibrahim, A. (2006). Comprehensive study of internal flow field and linear and nonlinear instability of an annular liquid sheet emanating from an atomizer. The dissertation submitted in partial fulfillment for the degree of Ph. D., University of Cincinnati.
17. Bruce, C. A. (1976) Dependence of ink jet dynamics on fluid characteristics. *IBM J. Res. Dev*., Vol. 1, p. 258.
18. Mansour, A. & Chigier, N. (1994). Effect of the turbulence on the stability of liquid jets and the resulting droplet size distributions. *Atomization Sprays*, Vol. 4, p. 583.
19. Lin, & Reitz, R. D. (1998). Drop and spray formation from a liquid jet. *Annu. Rev. Fluid Mech.*, Vol. 30, p. 85.
20. Kalaaji, A., Lopez, B., Attane, P. & Soucemarianadin, A. (2003). Breakup length of forced liquid jets. *Physics of Fluids*, Vol. 15, No. 9.
21. Sallam, K. A., Dai, Z. & Faeth, G. M. (2002). Liquid breakup at the surface of turbulent round liquid jets in still gases. *International Journal of Multiphase Flow*, Vol. 28, pp. 427-449.
22. Li, K. M. (2003). A predictive model for the initial droplet size and velocity distributions in sprays and comparison with experiments part. *Part. Syst. Charact*., Vol. 20, pp. 135-149
23. Movahednejad, E., Ommi, F., M.Hosseinalipour, S., Chen, C. P. & Mahdavi, S. A. (2011). Application of maximum entropy method for droplet size distribution prediction using instability analysis of liquid sheet. *Heat Mass Transfer*, Vol. 47, pp. 1591–1600.

APPENDIX

$$c_7\varpi^4+c_8\varpi^3+c_9\varpi^2+c_{10}\varpi+c_{11}+$$
$$-\frac{g_i\left(-c_1\varpi^4+c_{12}\varpi^3+c_{13}\varpi^2+c_{14}\varpi+c_{15}\right)}{c_{16}I_n\left(h\bar{k}_1\right)+\left(c_4-\varpi\right)\sqrt{1-\frac{c_5}{\left(c_4-\varpi\right)^2}}I_n'\left(h\bar{k}_1\right)}\left(c_4-\varpi\right)I_n\left(h\bar{k}_1\right)=0$$

$$c_1 = -B_n + g_0 G_n$$

$$c_2 = -2\left(n.\sqrt{\frac{We_s}{We_1}}+\bar{k}\right)B_n+$$
$$2\,g_0\left(n.\sqrt{\frac{We_{so}}{g_0 We_1}}+\bar{k}.\sqrt{\frac{We_o}{g_0 We_1}}\right)G_n$$

$$c_3=\frac{\bar{k}}{We_1}\left[\left(1-n^2-\bar{k}^2\right)+We_s-We_{so}\right]+$$
$$\left(n.\sqrt{\frac{We_s}{We_1}}+\bar{k}\right)^2 B_n-\left(n.\sqrt{\frac{We_{so}}{We_1}}+\bar{k}.\sqrt{\frac{We_o}{We_1}}\right)^2 G_n$$

$$c_4=\left(n.\sqrt{\frac{We_{si}}{g_i We_1}}+\bar{k}.\sqrt{\frac{We_i}{g_i We_1}}\right)$$

$$c_5=\frac{4\,We_{si}}{g_i We_1}$$

$$c_6 = \frac{\bar{k}}{h^2 We_l}\left(1 - n^2 - (h\bar{k})^2\right) + h\bar{k}\frac{We_{si}}{We_l} - \frac{\bar{k}}{h^3}\frac{We_s}{We_l}$$

$$c_7 = c_1 C_n - Q_n S_n$$

$$c_8 = -c_2 C_n - c_1 C_n b_3 + 2 b_1 Q_n S_n$$

$$c_9 = -c_3 C_n + c_2 C_n b_3 + c_1 C_n b_4 - 2 Q_n S_n b_2 - Q_n S_n b_1^2 + c_1 c_6$$

$$c_{10} = c_3 C_n b_3 - c_2 C_n b_4 + 2 Q_n S_n b_1 b_2 - c_2 c_6$$

$$c_{11} = -\left(c_3 C_n b_4 + Q_n S_n b_2^2 + c_3 c_6\right)$$

$$c_{12} = c_2 + 2 c_1 c_4$$

$$c_{13} = c_3 - 2 c_2 c_4 - c_1 c_4^2 + c_1 c_5$$

$$c_{14} = -2 c_3 c_4 + c_2 c_4^2 - c_2 c_5$$

$$c_{15} = c_3 c_4^2 - c_3 c_5$$

$$c_{16} = \frac{2n}{h\bar{k}}\sqrt{\frac{We_{si}}{g_i We_l}}$$

$$G_n = \frac{K_n(\bar{k})}{K'_n(\bar{k})}$$

$$B_n = \frac{I'_n(\bar{k}h)K_n(\bar{k}) - I_n(\bar{k})K'_n(\bar{k}h)}{I'_n(\bar{k}h)K'_n(\bar{k}) - I'_n(\bar{k})K'_n(\bar{k}h)}$$

$$C_n = \frac{I'_n(\bar{k})K_n(\bar{k}h) - I_n(\bar{k}h)K'_n(\bar{k})}{I'_n(\bar{k}h)K'_n(\bar{k}) - I'_n(\bar{k})K'_n(\bar{k}h)}$$

$$S_n = \frac{I'_n(\bar{k})K_n(\bar{k}) - I_n(\bar{k})K'_n(\bar{k})}{I'_n(\bar{k}h)K'_n(\bar{k}) - I'_n(\bar{k})K'_n(\bar{k}h)}$$

$$Q_n = -\left(\frac{I'_n(\bar{k}h)K_n(\bar{k}h) - I_n(\bar{k}h)K'_n(\bar{k}h)}{I'_n(\bar{k}h)K'_n(\bar{k}) - I'_n(\bar{k})K'_n(\bar{k}h)}\right)$$